Carbohydrate Polymers 200 (2018) 341–352

Contents lists available at ScienceDirect

Carbohydrate Polymers

journal homepage: www.elsevier.com/locate/carbpol

A novel pH-responsive hydrogel based on carboxymethyl cellulose/2-hydroxyethyl acrylate for transdermal delivery of naringenin

So Hyun Park, Hyuk Soo Shin, Soo Nam Park*

Department of Fine Chemistry, Cosmetic R&D Center, Cosmetic Industry Coupled Collaboration Center, Seoul National University of Science and Technology, 232 Gongneung-ro, Nowon-gu, Seoul 01811, South Korea

ARTICLE INFO

Keywords:
pH-responsive hydrogel
Carboxymethyl cellulose
2-Hydroxyethyl acrylate
Transdermal delivery system
Naringenin

ABSTRACT

In this study, a pH-responsive hydrogel (cl-CMC-g-pHEA), based on carboxymethyl cellulose/2-hydroxyethyl acrylate, was prepared. Its physicochemical properties and applicability as a transdermal delivery system for naringenin (NRG) were investigated. The hydrogel was synthesized *via* radical polymerization; its structure was analyzed by FT-IR and ^{1}H NMR. The water loss amount was measured by using thermogravimetric analysis; a porous 3D network structure was confirmed by SEM. All hydrogels showed greater swelling ratio at pH 7.5 and 8.5 than at pH 5.5. Rheological and texture analyses indicated a stable gel network and that grafting and crosslinking density influenced the mechanical properties of the hydrogel. The release behavior of NRG from the hydrogel could be explained by the Fickian diffusion mechanism. The hydrogel system enhanced transdermal delivery of NRG. Therefore, this novel pH-responsive cl-CMC-g-pHEA hydrogel may be useful as a transdermal delivery system for NRG and has potential applications in the treatment of atopic dermatitis.

1. Introduction

The skin is composed of three layers, namely the epidermis, dermis, and subcutaneous fat. The epidermis consists of the basal layer, spinous layer, granular layer, and the outermost layer, stratum corneum. The stratum corneum acts as a barrier to protect the skin from external stimuli and simultaneously blocks the passage of drug molecules (Michaels, Chandrasekaran, & Shaw, 1975; Otto & De Villiers, 2014; Park et al., 2018). Accordingly, various transdermal drug delivery systems (TDDS) have been developed to overcome the skin barrier and improve drug permeation efficiency. Hydrogels are chemically or physically cross-linked networks of hydrophilic polymers capable of absorbing large amounts of moisture (Dobić, Filipović, & Tomić, 2012). Hydrogels swollen with aqueous solutions have various applications, such as their use in tissue engineering, contact lens systems, and drug delivery systems due to their unique physical properties, particularly their thermodynamic stability (Das, Ghosh, Dhara, Panda, & Pal, 2015; Yu et al., 2017).

Transdermal drug delivery has been studied in patch systems containing various active ingredients (Boateng, Matthews, Stevens, & Eccleston, 2008; Wang, Hong, Chiu, & Fang, 2001). Hydrogels used in patches have an advantage due to their ability to locally seal the skin while hydrating the stratum corneum to promote absorption of the drug (Martin, Ladenheim, Marriott, Hollingsbee, & Brown, 2000). The transdermal permeability of a drug-containing hydro-patch system has been reported to be three to four times better than in non-sealed conditions (Ladenheim, Martin, Marriott, Hollingsbee, & Brown, 1996). It has also been reported that by hydrating the stratum corneum, most of the drug can be transmitted through the transdermal structures, such as the pores or sweat glands (Kwon, Kong, & Park, 2015).

Furthermore, hydrogels are classified as a "smart delivery system" because they are sensitive to various environmental conditions (temperature, pH, electrical current, and other such factors) depending on the nature of the functional groups (Puranik, Pao, White, & Peppas, 2016; Wei et al., 2015). The pH of the stratum corneum must be approximately 5.5 to maintain an effective barrier function and skin homeostasis. When the weakly acidic condition of the stratum corneum is altered, multiple skin diseases can be caused by the disturbance of the skin barrier and the consequent breeding of bacteria. In particular, the increased pH allows for skin dryness to occur, and this change in pH should be considered when formulating effective treatments. Therefore, attempts are being made to develop various pH-responsive hydrogels for the treatment of skin diseases (Koehler, Wallmeyer, Hedtrich, Goepferich, & Brandl, 2017; Kwon et al., 2015; Mauro et al., 1998).

Abbreviations: CMC, carboxymethyl cellulose; 2-HEA, 2-hydroxyethyl acrylate; KPS, potassium persulfate; PBS, phosphate buffer solution; PEGDA, poly(ethylene glycol) diacrylate; NRG, naringenin; TDDS, transdermal drug delivery system; TGA, thermogravimetric analysis; BG, 13-butylene glycol

* Corresponding author.
E-mail addresses: sh-cos@daum.net (S.H. Park), shs-cos@daum.net (H.S. Shin), snpark@seoultech.ac.kr (S.N. Park).

https://doi.org/10.1016/j.carbpol.2018.08.011
Received 20 March 2018; Received in revised form 16 July 2018; Accepted 4 August 2018
Available online 06 August 2018
0144-8617/ © 2018 Elsevier Ltd. All rights reserved.

Table 1
Synthesis details and gel fraction (%) of the cl-CMC-g-pHEA hydrogels.

Hydrogels	CMC (mol × 10^{-6})	2-HEA (mol × 10^{-2})	PEGDA (mol × 10^{-3})	KPS (mol × 10^{-5})	Water (mL)	Gel fraction (%)
cl-CMC-g-pHEA-1	5.56	3.05	0.32	1.85	50	61.7 ± 2.2
cl-CMC-g-pHEA-2	5.56	3.92	0.32	1.85	50	81.9 ± 1.8
cl-CMC-g-pHEA-3	5.56	4.79	0.32	1.85	50	74.2 ± 1.9
cl-CMC-g-pHEA-4	5.56	3.92	0.16	1.85	50	82.6 ± 4.1
cl-CMC-g-pHEA-5	5.56	3.92	0.48	1.85	50	79.2 ± 3.0

Biocompatible polymeric materials used for the production of hydrogels include cellulose, chitosan, and hyaluronic acid. Carboxymethyl cellulose (CMC), a chemical derivative of cellulose, is widely used owing to its high biodegradability, non-toxicity, and biocompatible properties. It contains a hydroxyl group (−OH) and a carboxyl group (−COOH) as functional groups, with the pKa of the carboxyl group being approximately 4.3. Therefore, this functional group is almost completely ionized under basic conditions and becomes progressively less ionized as the pH decreases, changing the physicochemical properties of the compound. Of all polysaccharides, CMC is easily available and it is also very cheap. (Liu, Zhai, Li, Peng, & Wu, 2002; Santa-Comba et al., 2001; Wach, Mitomo, Nagasawa, & Yoshii, 2003; Xiao & Gao, 2008). The compound 2-hydroxyethyl acrylate (2-HEA) is often used as a grafting agent to improve the adhesion and flexibility of CMC and to improve its mechanical properties (Tobing & Klein, 2001). 2-HEA is sometimes used as a material for contact lenses and is a biocompatible material (Chan, Wong, Byrne, Kavallaris, & Bulmus, 2008; Martínez-Ramos et al., 2008).

Naringenin (NRG), one of the major flavonoids found in citrus fruits, is known to have antioxidant, anti-inflammatory, anticancer, and antiproliferative effects (Chen, Chen, Cui, Yang, & Dou, 2007; Kawaii, Tomono, Katase, Ogawa, & Yano, 1999; Park, Kim, & Chio, 2012). According to a recent study, NRG treatment inhibited a Th1 immune reaction in 2,4-dinitrofluorobenzene-induced atopic dermatitis-induced mice, reduced infiltration of immune cells to skin lesion, and decreased IgE concentration in the blood, suggesting that it may be useful for treatment of atopic dermatitis (Karuppaqounder et al., 2016; Kim, Park, Kim, & Noh, 2013; Kim, Kim et al., 2013; Moon, Choi, & Kim, 2011). In addition, it has been reported that it possesses strong antibacterial activity against *Staphylococcus aureus*, which is detected in more than 90% of patients suffering from atopy (Mandalari et al., 2010; Rauha et al., 2000).

In this study, 2-HEA was grafted into CMC and crosslinked with poly (ethylene glycol) diacrylate (PEGDA) to produce a hydrogel for effective transdermal delivery of NRG. The concentration of the grafting agent and the crosslinking agent was adjusted to change the density of the polymer, and the physicochemical properties and transdermal permeability were accordingly investigated. The synthesis of the hydrogel was confirmed by Fourier transform infrared spectroscopy (FT-IR) and nuclear magnetic resonance (NMR), and the three-dimensional network structure was confirmed by scanning electronic microscopy (SEM). Thermogravimetric analysis (TGA), swelling ratio determination, and rheology and texture analysis were performed to investigate the physicochemical properties of the hydrogel. Drug release behavior at different pH was studied, and the kinetics and mechanisms of drug release were analyzed using several mathematical models. Finally, the possibility of application as a transdermal delivery vehicle for atopy and dry skin treatment was evaluated using a Franz diffusion cell.

2. Materials and methods

2.1. Materials

Sodium carboxymethyl cellulose (average Mw 90,000), 2-hydroxyethyl acrylate, poly (ethylene glycol) diacrylate (Mn 700), potassium persulfate (KPS), naringenin (NRG), and sodium phosphate dibasic dodecahydrate ($Na_2HPO_4{\cdot}12H_2O$) were purchased from Sigma-Aldrich (St. Louis, MO, USA). Sodium hydroxide (NaOH, assay = 98.0%) was purchased from OCI Co. Ltd. (Seoul, Korea). Sodium dihydrogen phosphate dihydrate ($NaH_2PO_4{\cdot}2H_2O$) was purchased from Junsei Chemical Co. Ltd. (Tokyo, Japan). Solvents, including 1,3-butylene glycol (1,3-BG), ethanol, and polyoxyl 60 hydrogenated castor oil (HCO-60), were of analytical grade. Milli Q water was used for all experiments.

2.2. Synthesis of cl-CMC-g-pHEA hydrogels

First, 50 mL of distilled water and CMC (5.56×10^{-6} mol) were placed in a 250 mL three-necked round-bottomed flask, and the mixture was stirred at 75 °C and 400 rpm in a water bath until the CMC was sufficiently dissolved. N_2 gas was then injected into the dissolved CMC solution for 20 min to sufficiently reduce the partial pressure of oxygen in the flask, and then KPS (1.85×10^{-5} mol) as a radical initiator was added and the mixture was left to react for 20 min. Next, a required amount of 2-HEA was added to the solution (Table 1). When the reaction mixture became milky white, the crosslinker PEGDA (Table 1) was added and the reaction was allowed to continue for another 3 h. Upon completion of the reaction, the compound was cooled sufficiently at room temperature. The stirring rate was adjusted during synthesis to induce homogeneous synthesis. The compound was dialyzed with 5 L of distilled water for 3 days or more to remove the unreacted crosslinking agent and monomers. Thereafter, the hydrogel was dried using a freeze dryer (-60 °C, 5 mm Torr; Ilshin Biobase, Seoul, Korea) for 3 days.

2.3. Gel fraction

The gel fractions of the hydrogels were measured through extraction in warm distilled water at 37 °C for 72 h. Next, they were dried in an oven at 60 °C for 72 h, until they reached a constant weight. The gel content was calculated according to Eq. (1) (Park & Nho, 2003).

$$\text{Gel fraction } (\%) = \frac{W_d}{W_i} \times 100 \quad (1)$$

W_i is the initial weight of the polymer and W_d is the dried gel weight after extraction.

2.4. FT-IR and ^{1}H NMR

The chemical structure of the synthesized hydrogel was confirmed using FT-IR and ^{1}H NMR spectroscopy. The FT-IR spectra of CMC, 2-HEA, PEGDA, and the dried hydrogel were obtained using an ATR-FTIR spectrometer (Travel IR, Smiths Detection, USA). The spectra were recorded in the range of 650-4000 cm^{-1} and 32 scans were obtained by using a Smart Orbit ATR accessory with a diamond crystal and Omnic 8.0 software. The ^{1}H NMR spectra were detected with a nuclear magnetic resonance (NMR) spectrometer (Model: DD2 700, Agilent Technologies-Korea, USA). The HR-MAS NMR spectra (proton) of the synthesized hydrogel were obtained using a 700 MHz FT-NMR spectrometer (Bruker, Rheinstetten, Germany). The spin rate was 6000 Hz, the temperature was 298 K, the probe used high-resolution magic angle

spinning, and the recycle delay time was 4 s.

2.5. Morphology

Morphological observations of the dried hydrogels were performed. The three-dimensional network structure of the hydrogel was confirmed using SEM (Tescan Vega 3, Tescan, Czech) with an acceleration voltage of 15 kV. The dried hydrogel was observed after sputtering with Pt, the voltage was adjusted to 1.0–1.5 kV at the time of measurement, and each sample was photographed at ×500 magnification. The pore size was measured by using the ImageJ software.

2.6. Thermogravimetric analysis

The thermogravimetric analysis of the swollen hydrogel was measured using a JP/DTG-60 (Shimadzu, Tokyo, Japan). After excessive water on the gel surface was removed with filter paper, a piece of approximately 20 mg of weight was cut off and weighed accurately. The analysis was then carried out under N_2 with a flow rate of 50 mL/min, at a heating rate of 3 °C/min in a temperature range of 20–220 °C. The standard material used was alumina powder.

2.7. Swelling study and its kinetics

The swelling ratio of the cl-CMC-g-pHEA hydrogels was measured by changing the pH. The synthesized hydrogels were cut into similar sizes (5 mm × 5 mm × 2 mm) and equal weight (0.2 ± 0.01 g). Individual pieces were then put into a phosphate buffer solution (PBS) at different pH values (pH = 5.5, 7.5, and 8.5). After swelling for 24 h at 37 °C to simulate the body temperature and application of biomedicals, swelled hydrogels were taken out, excess solvent on the surface was gently removed, and then the swelled hydrogels were weighed. The swelling ratio was calculated according to Eq. (2).

$$Swelling\ ratio\ (\%) = \frac{W_s - W_d}{W_d} \times 100 \quad (2)$$

W_s is the weight of swollen hydrogel (g) and W_d is the weight of dried hydrogel (g).

For swelling kinetics, water absorption of the hydrogels was measured at consecutive time intervals until and unless equilibrium was achieved. The pH-sensitivity of the hydrogel was determined using the equilibrium swelling ratio in various buffer media. The Voigt model (Eq. (3)) was used to determine the swelling rate of the hydrogels.

$$S_t = S_e\left(1 - e^{-t/\tau}\right) \quad (3)$$

S_t (g g^{-1}) is the swelling at time t, S_e (power parameter, g g^{-1}) is the equilibrium swelling, t is the time (min) for swelling, and τ (min) stands for the rate parameter. For calculating the rate parameter, by using Eq. (3), one can plot $\ln(1-S_t/S_e)$ *versus* time (t). The slope of the fitted straight line *slope* = $1/\tau$ gives the rate parameter (Anirudhan, Sandeep, & Divya, 2012).

2.8. Rheological characteristics

The rheological properties of the cl-CMC-g-pHEA hydrogel were measured at 37 °C using a Thermo Haake MARS rheometer (Thermo Electron GmBH, Karlsruhe, Germany), which had a 35-mm diameter parallel plate geometry. Samples were 2-mm thick and cut into the diameter size of the probe. Frequency sweep measurement was executed with a range of 10^{-2}-10^{-1} Hz. To find out the yield stress, amplitude sweep was performed with a variation of shear stress (from 10 to 1000 Pa) at 1 Hz. Shear viscosity of the gel samples was measured between the shear rate range of 1–500/s.

2.9. Texture analysis

A texture analyzer (TA.XT Express Enhanced, Stable Micro Systems, Godalming, Surrey, UK) was used to analyze texture properties of hydrogels. Samples were 1-cm thick and cut into the size of the probe's diameter. For the load cell, a force up to 5-kg could be measured and a 40-mm disc probe was compressed twice consecutively into the hydrogel. The trigger load was fixed at 5.0 g, the strain was 30%, the probe speed was fixed at 2.0 mm/s, and the probe was positioned above the gel surface. From the resultant force-distance curve, hydrogel hardness, cohesiveness, resilience, chewiness, adhesiveness, and springiness of the formulations were calculated using the Texture Exponent 32 software (Kong, Kim, & Park, 2016; Kwon et al., 2015).

2.10. In vitro cytotoxicity

Cytotoxicity was assessed using the MTT assay to determine the toxicity of hydrogels to the skin. The cl-CMC-g-pHEA hydrogels (1 × 1 cm) were eluted into DMEM supplemented with 10% FBS, penicillin 100 U mL^{-1} and streptomycin 100 μg mL^{-1} at 37 °C for three days and seven days to obtain an eluate. HaCaT cells were seeded at a density of 1 × 104 cells/well in a 96-well plate and cultured *in vitro* at 5% CO_2 and 37 °C for one day, after which the eluate was dispensed to the cells. The cytotoxicity was evaluated by comparing the survival rate of HaCaT cells in the presence and absence of the hydrogels using the MTT assay. The absorbance was measured at 570 nm using an ELISA reader (Tecan, Austria). The absorbance of the untreated group was determined as a negative control (100%) and the relative cell viability of the treated group was determined according to Eq. (4) (Kim, Park, Kim, & Noh, 2013).

$$Cell\ viability\ (\%) = \frac{A_{treated\ group}}{A_{untreated\ group}} \times 100 \quad (4)$$

2.11. Drug release study of the cl-CMC-g-pHEA hydrogel

2.11.1. Drug release behavior

Dried hydrogel (100 mg) was immersed in 20 mL of a 20% 1,3-BG in PBS containing 0.5 mM NRG in order to measure the drug incorporating efficiency of the hydrogel. The resultant NRG-loaded hydrogel was incubated at 37 °C for 24 h. After the hydrogel was removed from the solution, the surface liquid was removed. Incorporating efficiency was determined *via* UV/vis spectroscopy using an NRG calibration curve. The absorbance was measured at the maximum absorption wavelength of NRG, λ_{max} = 292 nm. The amount of drug incorporated into the hydrogel was calculated according to Eq. (5).

$$Drug\ incorporating\ efficiency\ (\%) = \frac{V_1C_1 - V_2C_2}{V_1C_1} \times 100 \quad (5)$$

V_1: the volume of initial NRG solution (mL)
V_2: the remaining volume of the NRG solution (mL)
C_1: the initial concentration of NRG (mM)
C_2: the final concentration of NRG (mM)

Drug release behavior was assessed using PBS at various pH (pH = 5.5, 7.5, and 8.5). The NRG-loaded hydrogel was immediately immersed in the release medium (PBS with 20% 1,3-BG) and released at 37 °C. Release medium (0.5 mL) was taken at a constant time and a fresh medium (0.5 mL) was added to maintain a constant volume. The *in vitro* release study was performed for 24 h. Drug concentration was analyzed using an analytical calibration curve of NRG with UV/vis spectroscopy.

2.11.2. Drug release kinetics and mechanism

The *in vitro* drug release mechanism of the hydrogel can be explained by the erosion of the network structure and the diffusion of NRG. This mechanism can be modeled with first-order, Hixson-Crowell,

and Higuchi equations. The equation was calculated using Polymath professional 6.1 and the best model was the one with the highest correlation coefficient (R^2). The mechanism of drug release can be inferred based on the equation to involve diffusion, corrosion, and binding mechanisms. The model equations are as follows (Dash, Murthy, Nath, & Chowdhury, 2010).

First-order model:

$$M_t = 1 - e^{-K_1 t} \quad (6)$$

Hixson-Crowell model:

$$M_t = 1 - (1 - K_{HC} t)^3 \quad (7)$$

Higuchi model:

$$M_t = K_H t^{1/2} \quad (8)$$

M_t is the fraction of drug released at each time point (t) and K_1, K_{HC} and K_H represent the first-order release kinetic constant, the Hixson-Crowell release kinetic constant, and the Higuchi release kinetic constant, respectively.

In addition, since the release mechanism from polymeric systems is complex, the Korsmeyer-Peppas model was used to determine whether more than one release mechanism was involved and to determine the exact mechanism of drug release (Korsmeyer, Gurny, Doelker, Buri, & Peppas, 1983).

Korsmeyer-Peppas model:

$$M_t = Kt^n \quad (9)$$

K is a kinetic constant incorporating structural and geometric characteristics of the device, and n is the release exponent, indicative of the mechanism of drug release. The release mechanism could be characterized by the value of n, the release exponent. The case of $0.45 \geq n$ corresponds to Fickian diffusion (diffusion-controlled drug release), $0.45 < n < 0.89$ corresponds to non-Fickian transport, $n = 0.89$ corresponds to Case II transport (erosion-controlled drug release), and $n > 0.89$ to corresponds to super case II transport mechanism. When determining n, only the portions of the release curve where $M_t \leq 60\%$ were used.

Analysis of the results of all experiments (100% release curves) was done using the model proposed by Peppas and Sahlin. This was proposed to explain not only the diffusion but also the relaxation effect of the polymer in the release mechanism of the drug from the polymer matrix (Peppas & Sahlin, 1989).

Peppas-Sahlin model:

$$M_t = K_f t^m + K_r t^{2m} \quad (10)$$

The value of m in our study was based on the aspect ratio of the matrices. K_f and K_r are constants representing the relative contributions of drug diffusion and polymer relaxation to drug release.

2.12. In vitro skin permeation

The *in vitro* skin permeation study of the NRG-loaded cl-CMC-g-pHEA hydrogel was carried out using Franz diffusion cells (Permegear, USA). The skin was removed from a hairless mouse (6 weeks, female) after careful removal of the subcutaneous fat and excess tissue. Between the donor and the receptor phases, the stratum corneum was placed face-up and the skin was fixed. The sample was uniformly applied on a 0.6362 cm^2 area of the skin. The receptor chamber was filled with receptor phase (HCO-60:EtOH:PBS = 2:20:78 (v/v%)) and stirred at 150 rpm for 24 h. The temperature was maintained at 37 °C in a constant temperature water bath.

Samples (0.1 ml) of identical concentration were applied to the skin in the donor compartment and the amount of hydrogel was determined by considering the incorporating efficiency of NRG. The receptor phase was collected through the sampling port after 24 h. To measure the amount of NRG contained in the skin, the surface of the skin was cleaned with PBS. The stratum corneum was removed 3 times by stripping with 3 M scotch tape (3 M, Korea). After which, NRG in the skin and the tape were dissolved in 100% ethanol by sonication. The concentration of NRG was determined *via* UV/vis spectroscopy.

2.13. Drug stability

The stability study of the NRG-loaded cl-CMC-g-pHEA hydrogel was performed for 30 days to determine the effect of environmental factors, such as temperature, humidity, and light, on drug-release characteristics. Hydrogels were stored in an incubator (Model: *J*-HRC1B, Jeil Scientific Ind. Co., Korea) and maintained at a temperature of 40 ± 2 °C and relative humidity (RH) of 75 ± 5% throughout the study period (Das & Pal, 2015).

3. Results and discussion

3.1. Synthesis of the cl-CMC-g-pHEA hydrogel

The cl-CMC-g-pHEA hydrogel developed in this study was synthesized by radical polymerization using PEGDA and KPS as crosslinking agents and initiators, respectively. PEGDA has been used in many studies as a biocompatible polymer with low toxicity (Demirdirek & Uhrich, 2017; Zhang, Yang, & Nie, 2008; Zhong, Wu, Reinhart-King, & Chu, 2010). The radical reaction can be divided into three stages of initiation, propagation, and termination. In the initiation, KPS generates radicals in the CMC under thermal conditions. In the propagation, radicals generated in CMC induce polymerization of 2-HEA monomers and PEGDA. Finally, after all the generated radicals have reacted, the radical reaction is terminated. The hydrogel was prepared with different concentrations of grafting agent and crosslinking agent. Its composition and gel fraction are shown in Table 1.

3.2. FT-IR and ^{1}H NMR

FT-IR was used to confirm the synthesis of the hydrogel, allowing for clear functional group analysis of the organic molecules. Therefore, the FT-IR spectra of the network system of the cl-CMC-g-pHEA hydrogel were compared with FT-IR spectra of CMC, 2-HEA, and PEGDA (Fig. 2a). Peaks at 1631 and 1635 cm^{-1} in the 2-HEA and PEGDA spectra were due to the presence of a C=C double bond conjugated with an ester (−COO-). The hydrogel spectra showed that the peak corresponding to the conjugated C=C double bond (1600-1650 cm^{-1}) disappeared, suggesting that the double bond found in 2-HEA and PEGDA was reduced by a radical reaction. Based on these results, it was confirmed that the hydrogel was well-synthesized.

In addition, the broad peak at 3500-3300 cm^{-1} was due to the stretching vibration of −OH, and the peaks at 2950 cm^{-1} and 2884 cm^{-1} represented asymmetric and symmetric stretching vibrations of methylene C–H. Peaks at 1723 and 1720 cm^{-1} were due to the stretching vibration band of the ester C=O, and that at 1396 cm^{-1} was caused by the symmetric stretching vibration band of carboxylate (−COO-) in CMC. The peaks at 1246 cm^{-1} and 1165 cm^{-1} indicated the stretching vibrations of the ester C–O. These peaks appeared at lower frequencies (1276 cm^{-1} and 1195 cm^{-1}) in the hydrogel spectra, representing the ester C–O in 2-HEA and PEGDA because the double bond of the α, β-unsaturated ester (−C=C−COO−) disappeared in the hydrogel and the ester C–O bond strength decreased.

Fig. 2b shows the ^{1}H NMR spectra of CMC, 2-HEA, and PEGDA, as well as the ^{1}H HR-MAS NMR spectrum of the cl-CMC-g-pHEA hydrogel. In the ^{1}H NMR spectrum of CMC, an anomeric proton (H1) was observed at 4.576 ppm, whereas other protons (H2-H7) in the glucose ring and additional methylene protons in the substituted carboxymethyl groups overlapped in the narrow region 3.395–4.310 ppm (Bisht, Pandey, Joshi, & Naithani, 2017; Yáñez-S et al., 2018). In the case of 2-HEA, the chemical shifts between δ = 6.527–6.553, 6.288–6.328, and

6.076–6.091 ppm are due to protons associated with unsaturated carbons, *i.e.* for H8, H9, and H8′, respectively. The chemical shifts at δ = 3.925–3.929 and 4.349–4.353 ppm are due to the protons of position H10 and H11, respectively (Das, Pham, & Noh, 2018). For PEGDA, the chemical shifts appeared for the unsaturated protons between δ = 6.526–6.551, 6.289–6.330, and 6.090–6.105 ppm, *i.e.* for H12, H13, and H12′, respectively. On the other hand, the chemical shifts between δ = 3.770–3.803, 3.900, and 4.427 ppm are caused by the protons of H14/H15, H16, and H17, respectively (Das et al., 2018). In the ^{1}H HR-MAS NMR spectrum of the cl-CMC-g-pHEA hydrogel, the chemical shifts between δ = 4.486, 4.210–4.217, 3.455, and 3.302 ppm are due to anomeric protons (H1) and other protons (H2-H7) in the ring and additional methylene protons of the CMC unit. The chemical shifts at δ = 3.593–3.599, 3.738, 3.854, 4.022, and between 4.116–4.146 ppm are caused by H17, H10/H18, H8, H12 and H11/H19 protons, respectively. The chemical shifts between δ = 1.609–1.746, 1.949–1.956, 2.384, and 2.458 ppm are due to H13, H15, H9/H14, and H16 protons, respectively. In the NMR spectrum of the synthesized hydrogel, no chemical shifts appeared between δ = 6.076–6.553 ppm (for unsaturated protons). Instead, new chemical shifts appeared between δ = 1.609–2.458 ppm, which confirmed that 2-HEA and PEGDA were also polymerized in the reaction medium. The chemical shift at δ = 3.854 (H8) ppm signified the covalent attachment between CMC and poly(2-HEA), which also verified the grafting of poly(2-HEA) onto the hydroxyl groups of CMC (Das et al., 2018).

On the other hand, the absence of chemical shifts of unsaturated protons in PEGDA and the appearance of new chemical shifts at δ = 1.949–1.956 and 2.458 ppm ascertained that PEGDA crosslinked two graft polymers of CMC and poly(2-HEA), as well as formed crosslinked cl-CMC-g-pHEA hydrogel (Fig. 1).

The grafting degree of poly(2-HEA) in the hydroxyl groups of CMC can be quantitatively calculated through the integration ratio of hydroxyl protons (H12) of 2-HEA at 4.022 ppm and the ring protons (H2) of CMC unit at 3.302 ppm using Eq. (11) (Yao et al., 2014).

$$\textit{Grafting degree}\ (\%) = \frac{I_{H12}}{I_{H2} * 2} \times 100 \tag{11}$$

The grafting degree of the cl-CMC-g-pHEA-4 hydrogel was 44. 5% in, assuming that I_{H2} (base value for one proton of CMC) = 1.00 and I_{H12} (for two protons of 2-HEA) = 0.89. Moreover, the grafting degree (%) of all hydrogels are reported in Fig. S1, in which cl-CMC-g-pHEA-3 exerted the highest grafting degree.

The crosslinking density has been determined using the intensities of the characteristic peaks of 2-HEA (H13) and PEGDA (H17). The intensity of H13 protons, which was formed during the polymerization of 2-HEA, should be the same as that of H17 protons of PEGDA. Thus, the crosslinking density was calculated according to Eq. (12) (Arunbabu, Shahsavan, Zhang, & Zhao, 2013; Patra et al., 2018):

$$\textit{Crosslinking density}\ (\%) = \frac{I_{H17}}{I_{H13}} \times 100 \tag{12}$$

The crosslinking density of the cl-CMC-g-pHEA-4 hydrogel was 27.0% (assuming I_{H13} = 19.98 and I_{H17} = 5.40). Furthermore, the crosslinking density (%) of all hydrogels are reported in Fig. S1, in which cl-CMC-g-pHEA-5 had the highest crosslinking density.

3.3. Morphology

We confirmed a three-dimensional crosslinking network in the dried hydrogel using SEM. SEM analysis revealed the flaked particle morphology of CMC (See Fig. S2). After crosslinking on CMC using 2-HEA as a monomer and PEGDA as a crosslinker, the cl-CMC-g-pHEA hydrogels showed a porous structure (See Fig. 3). We calculated the pore sizes using the ImageJ software and the results showed that the largest to smallest pore sizes belonged to: cl-CMC-g-pHEA-1 (40–89 μm) > cl-CMC-g-pHEA-4 (33–56 μm) > cl-CMC-g-pHEA-2 (26–54 μm) > cl-CMC-g-pHEA-3 (12–26 μm) > cl-CMC-g-pHEA-5 (12–22 μm). As the concentrations of the grafting agent and the crosslinking agent increased, the pore size decreased. In the concept of bound water and free water, as the pore size increases, the proportion of bound water decreases and the proportion of free water increases. Therefore, as the concentration of grafting agent and crosslinking agent decreases, the pore size increases, so that the incorporating efficiency of the drug solution carrying the active ingredient is increased and transdermal delivery is more efficient (Pasqui, De Cagna, & Barbucci, 2012).

Hydrogels can be classified into four types according to the size and structure of their pores (Ganji, Vasheghani-Farahani, & Vasheghani-Farahani, 2010). The types are as follows: micro-porous with no pores, micro-porous with pore diameters of 100–1000 Å, macro-porous with pore diameters of 0.1–1 μm, and super-porous with pore diameters greater than 1 μm. Non-porous, microporous, and macroporous hydrogels are all closed structures with no inter-connections between the pores. In contrast, the cl-CMC-g-pHEA hydrogel was found to be a super-porous hydrogel (SPH), with larger diameter pores and an open cell structure with interconnections between the pores. SPH is a capillary system that captures moisture quickly inside the pores and is widely used for drug delivery system (DDS) (Dorkoosh et al., 2002; Ganji et al., 2010).

3.4. TGA analysis

TGA analysis measures characteristics, including thermal stability, and water content of multiple component substances by measuring the mass changes of substances with temperature. In particular, water content is a critical feature in the field of transdermal drug delivery.

The TGA curve in this study was used to evaluate the water evaporation rate of the cl-CMC-g-pHEA hydrogels. All hydrogels showed similar curves with decreasing mass from 20 to 140 °C (see Fig. S3). This phenomenon is caused by the evaporation of water in the hydrogel. Water loss occurred at such high temperature because of the powerful hydrogen bonds between water and the polymer chains in the hydrogel (Weian, Wei, & Yue'e, 2005). At 100 °C, the mass losses were cl-CMC-g-pHEA-1 (-95.3%) > cl-CMC-g-pHEA-4 (-90.3%) > cl-CMC-g-pHEA-2 (-87.6%) > cl-CMC-g-pHEA-3 (-81.5%) > cl-CMC-g-pHEA-5 (-79.2%). These results indicated that an increase in 2-HEA and PEGDA resulted in lower evaporation rates. This is explained by considering that the 2-HEA and PEGDA polymer chain has hydrogen bonds with water, which decreases the amount of water lost from the hydrogel (Guo, Wistrand, & Albertsson, 2011; Kwon et al., 2015).

3.5. Swelling study and its kinetics

Hydrogels generally swell when exposed to external solvents. These swelling behaviors are mainly related to osmotic pressure, the electrostatic force, and a viscoelastic restoring force (Peppas & Hoffman, 2013). Two important factors in the swelling kinetics and ratio of a hydrogel are the pore size and pore structure.

In order to confirm whether the hydrogel exhibited a pH-responsive swelling behavior, a swelling study was carried out at pH 5.5 (the normal skin pH), 7.5 (the acne skin pH), and 8.5 (the atopic skin pH) (Fig. 4). It was also apparent that the swelling ratio of all hydrogels was higher at pH 7.4 and 8.5 than at pH 5.5. These results are due to the ionization of the carboxyl group of CMC and the proton balance. At pH 5.5, most of the carboxyl groups are protonated and strong hydrogen bonds between them cause dominant polymer-polymer interactions over polymer-water interactions. At pH 7.5 and 8.5, the carboxyl group ionized and the electrostatic repulsion between them extended the network further and increased the swelling ratio of the hydrogel. The cl-CMC-g-pHEA hydrogel was found to follow the Henderson-Hasselbalch equation, which expresses the extent of ionization of a hydrogel in the swelling medium. However, at pH 8.5, the swelling ratio decreased slightly more than at pH 7.5. The reason for this phenomenon is that the

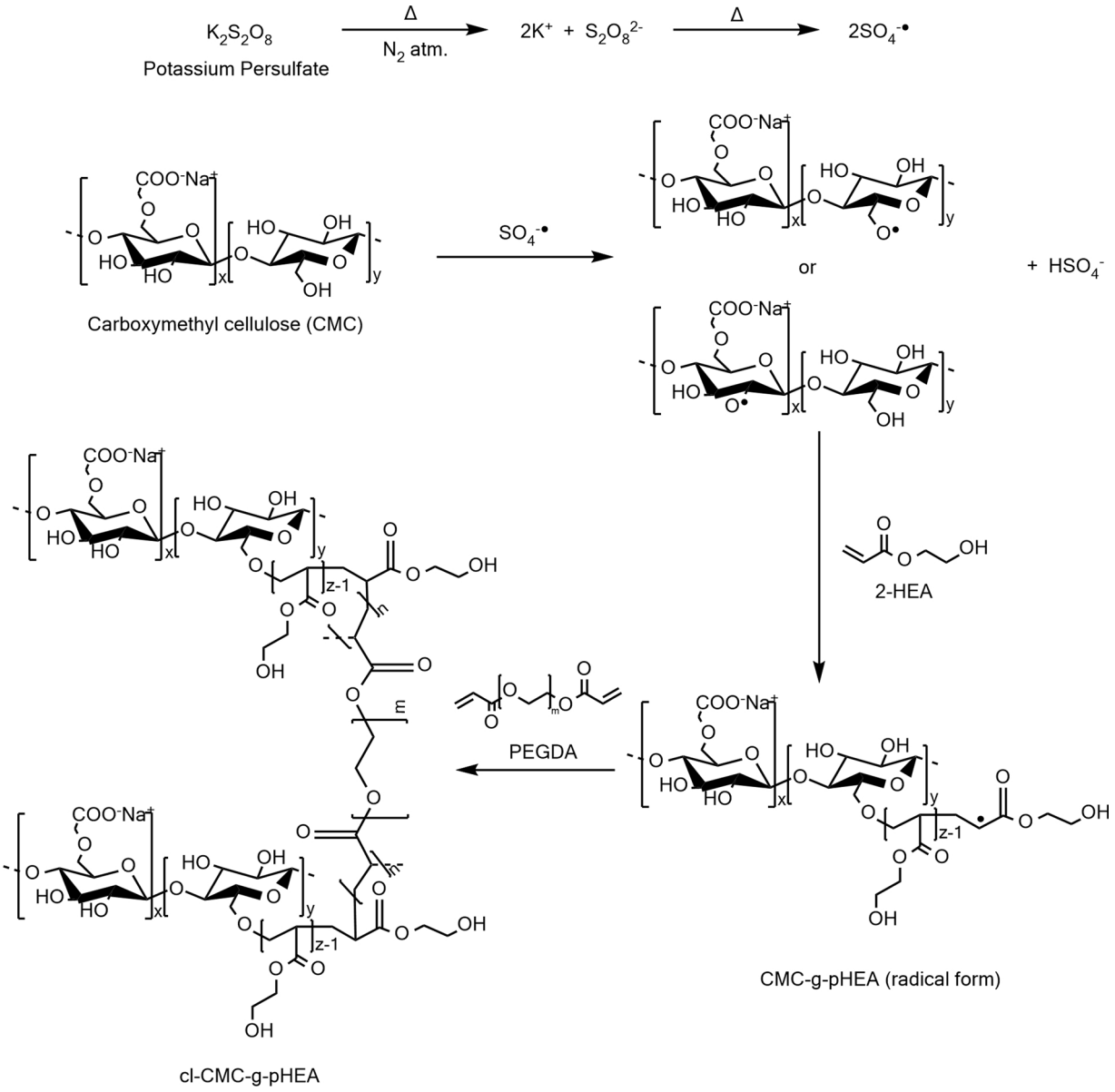

Fig. 1. Probable reaction mechanism for the synthesis of cl-CMC-g-pHEA hydrogels.

excess Na^+ in the swelling media caused a "charge screening effect," which shielded the carboxylate anions and prevented electrostatic repulsion (Devi & Narzary, 2012; Hu et al., 2017).

The influence of the concentration of the grafting agent and the crosslinking agent on the swelling ratio can also be seen in Fig. 4. As the content of 2-HEA and PEGDA increased, the swelling ratio decreased. High grafting and crosslinking density result in dense gel structures that reduce the swelling ratio, restrict the repulsion force between chains, and slow permeation of the medium. Additionally, in the lower 2-HEA and PEGDA concentration, the difference in swelling at pH 5.5 and pH 7.5 was more apparent. The expansion of pores is limited in dense networks, leading to decreased pH sensitivity (Kong et al., 2016).

The rate of water diffusion in the hydrogel network at pH 5.5, 7.5, and 8.5 was calculated using the Voigt model (Table S1). The characteristics rate parameter (τ) value shows the rate of swelling. For the cl-CMC-g-pHEA-4 hydrogels, the rate parameter (τ) was lower at pH 7.5 (~134) and 8.5 (~139) than at pH 5.5 (~157). This decrease in rate parameter of hydrogel with an increase in pH indicated that hydrogels become more fast-swelling at alkaline pH than at acidic pH (Anirudhan, Sandeep, & Divya, 2012).

3.6. Rheological characteristics

Rheological property data provide information regarding the elasticity and viscosity of the hydrogel quickly and accurately (Anseth, Bowman, & Brannon-Peppas, 1996; Zuidema, Rivet, Gilbert, & Morrison, 2014). Fig. 5a shows the frequency independent storage modulus G′ and loss modulus G″ of the cl-CMC-g-pHEA-4 hydrogel, which had the highest gel fraction. In gels, it is known that G′ is independent of frequency and storage modulus is higher than loss modulus (Bonacucina, Martelli, & Palmieri, 2004). The cl-CMC-g-pHEA hydrogel showed gel characteristics. On the basis of the amplitude sweep measurement (Fig. 5b and Fig. S4), it was obvious that G′ remains higher than G″ at a certain limit of shear stress. This clearly indicated the gel characteristics of all synthesized hydrogels. Moreover, after a certain shear stress, both G′ and G″ decreased rapidly because of the breakdown of the crosslinked network of the hydrogel. This shear stress is called yield stress (σ) (Mandal, Rameshbabu, Dhara, & Pal, 2017). The yield stress (σ) and gel strength (G′/G″) values of all hydrogels are reported in Table S2, in which cl-CMC-g-pHEA-5 had highest σ value, indicating the strongest gel network. Additionally,

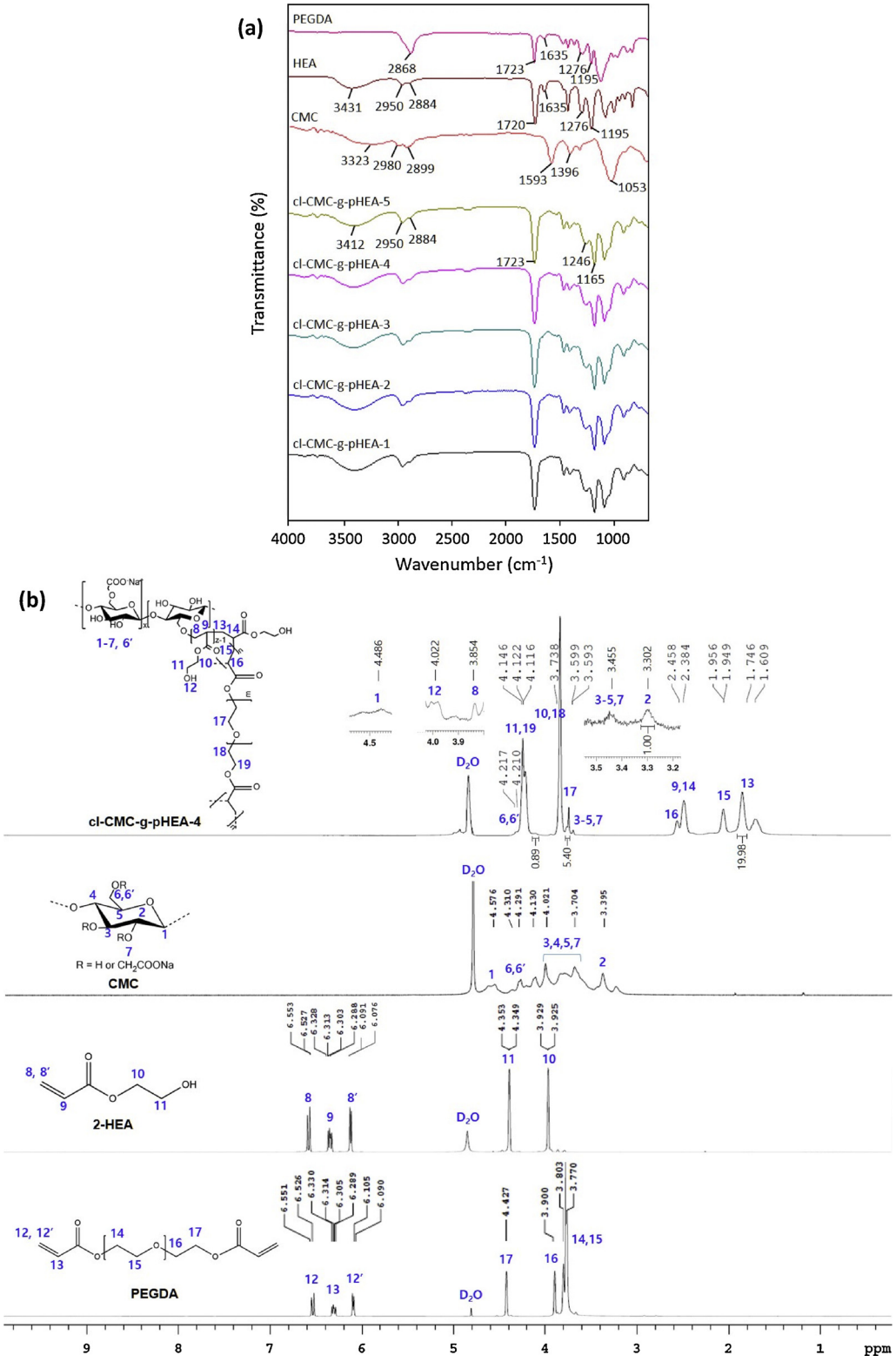

Fig. 2. (a) FT-IR spectra of CMC, 2-HEA, PEGDA, and cl-CMC-g-pHEA hydrogels and (b) ^{1}H NMR spectra of CMC, 2-HEA, and PEGDA, as well as the ^{1}H HR-MAS NMR spectrum of the cl-CMC-g-pHEA-4 hydrogel.

Fig. 5c displays a continuous decreasing trend of shear viscosity with increasing shear rate, which indicated the shear thinning behavior of cl-CMC-g-pHEA-4 (Das et al., 2015).

3.7. Texture analysis

Skin can exhibit dynamic motion. Therefore, when a hydrogel is used as a transdermal delivery system, intimate contact is required between the gel and the skin so that the gel remains adhered to the skin even during skin movement (Hurler, Engesland, Kermany, & Škalko-

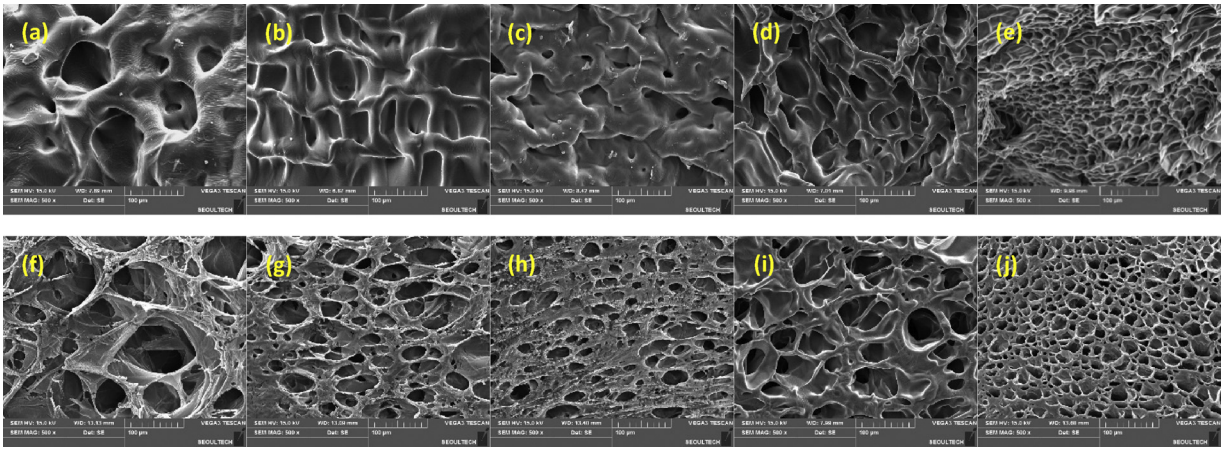

Fig. 3. SEM images of the surface (a, b, c, d, e), and cross-section (f, g, h, i, *j*) morphology of freeze-dried cl-CMC-g-pHEA-1, 2, 3, 4, 5 hydrogels, respectively. Scale bars represent 100 μm (Magnification = 500×).

Basnet, 2012). Hardness can indicate the applicability of the hydrogel to the skin and adhesiveness can be an indicator of the duration at the skin application site. These properties are directly related to polymer concentration and composition (Jones, Woolfson, & Brown, 1997). Texture analysis provides reliable information about these properties.

The gel hardness, cohesiveness, resilience, chewiness, adhesiveness, and springiness of cl-CMC-g-pHEA hydrogels are shown in Fig. 6. As the grafting percentage increased, the hardness and cohesiveness also increased (cl-CMC-g-pHEA-1 < cl-CMC-g-pHEA-2 < cl-CMC-g-pHEA-3). As the proportion of crosslinks increased, the hardness and cohesiveness also increased (cl-CMC-g-pHEA-4 < cl-CMC-g-pHEA-2 < cl-CMC-g-pHEA-5). Apparently, an increase in the ratio of grafting and crosslinking caused the hydrogel network to be tightly entangled at the time of formation, resulting in a hard and cohesive gel structure. Therefore, a low ratio of grafting and crosslinking resulted in the formation of a loose structure. Resilience and chewiness showed the same tendency as hardness and cohesiveness. In particular, cl-CMC-g-pHEA-1 had the least amount of 2-HEA which improves its elasticity, so caused it to show very low resilience. Chewiness was closely related to hardness because it equaled hardness × cohesiveness × springiness values.

Adhesiveness can occur due to a dehydration effect by hydrophilic functional groups such as −OH (Xu et al., 2014). The cl-CMC-g-pHEA hydrogels had decreased adhesiveness when the polymer and crosslinking density were increased. This may be due to the fact that adhesiveness to the other surfaces decreases as attraction inside the gel increases. However, in this study, adhesiveness result could not be explained only through the attraction between the gel surface and the probe surface. During the withdrawal process, a small piece of the gel was stuck to the probe and was separated from the original gel sample. In this way, the adhesiveness was closely related not only to the adhesion to the probe surface but also to the cohesion of the gel itself (Xu et al., 2014). Thus, in order to produce an optimal transdermal delivery system, the gel must have a balance of adhesion and cohesiveness in order to prolong the duration at the hydrogel application site. On the other hand, the springiness (the gel height after pressing/the gel height before pressing) was close to 1 with almost no difference between the samples.

3.8. *In vitro cytotoxicity*

Cytotoxicity is one of the most important indexes for the practical application of hydrogel. In this study, we evaluated the cytotoxicity of cl-CMC-g-pHEA hydrogels in HaCaT cells using the MTT assay (see Fig. S5). All hydrogels and the negative control group showed similar cellular activity after 24 h of incubation. There was no significant difference in cell growth profiles between cells grown in different extract

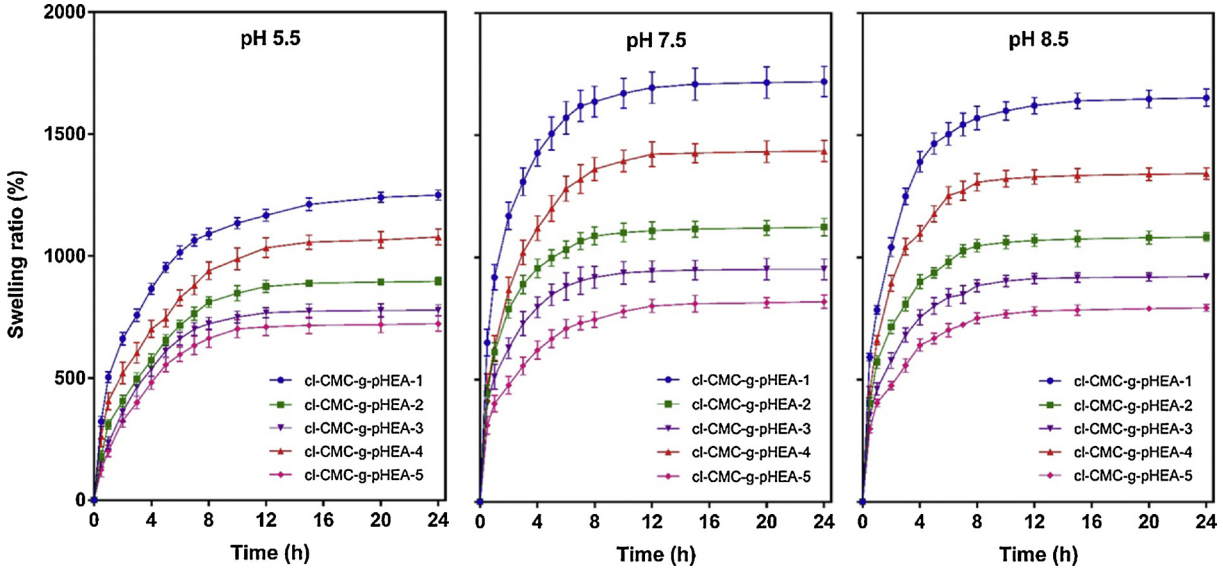

Fig. 4. Swelling ratio (%) for cl-CMC-g-pHEA hydrogels in pH 5.5, 7.5, and 8.5, as determined using Eq. (2). Values are presented as mean ± SD (n = 3).

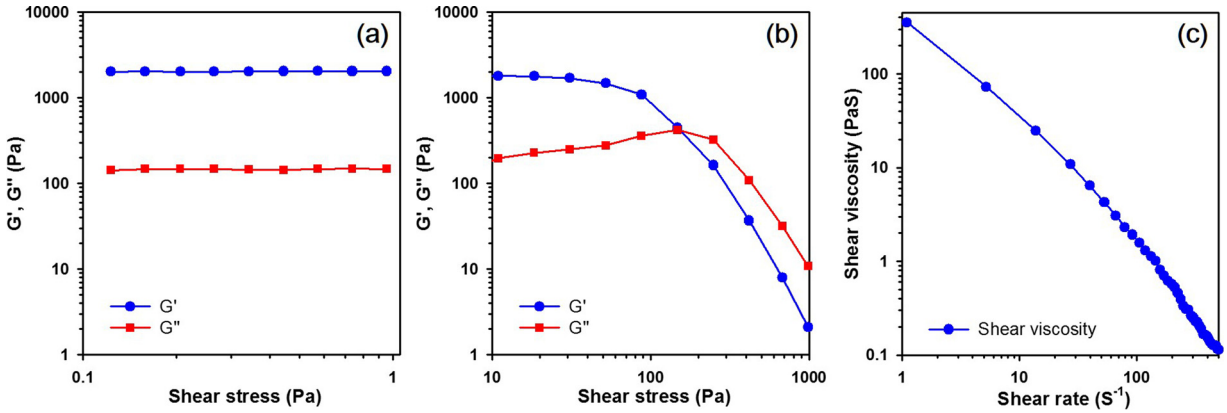

Fig. 5. Plots of (a) G′, G″ *vs* frequency, (b) G′, G″ *vs* shear stress, and (c) shear viscosity *vs* shear rate of the cl-CMC-g-pHEA-4 hydrogel.

media (3 days and 7 days). All samples exhibited cell viability of over 90%. These results suggested that the cl-CMC-g-pHEA hydrogels were nontoxic to HaCaT cells.

3.9. In vitro drug release

The cl-CMC-g-pHEA-4 hydrogel was chosen as the optimal material for application as a transdermal delivery system based on its high gel fraction, excellent adhesion, and proper cohesion. Therefore, we examined the drug release behavior from this gel at pH 5.5 (the normal skin pH), 7.5 (the acne skin pH), and 8.5 (the atopic skin pH). The NRG solution was inserted into the hydrogel matrix *via* the swelling method. The incorporating efficiency of NRG was 51.5% after 24 h (see Fig. S6), and the amount released was calculated relative to this. The cumulative release of drug at pH 5.5, 7.5, and 8.5 after 24 h was 42, 70, and 73%, respectively (Fig. 7). The drug release rate was consistent with the swelling value. This suggested that pH may affect drug release in a cl-CMC-g-pHEA hydrogel system and that NRG release will be easier in the basic skin such as atopic skin.

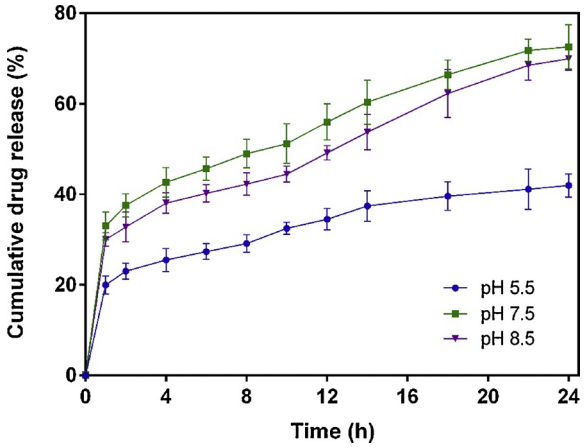

Fig. 7. *In vitro* drug release profiles of cl-CMC-g-pHEA hydrogels with different pH levels. Values are presented as mean ± SD (n = 3).

As shown in Fig. 7, initial releases were all rapid. This occurs since the crosslinked network of the porous hydrogel cannot control the surface drug release when it is exposed to the release medium which allows free initial dissolution of the drug (Kong et al., 2016). The amount of drug released continued to increase over time. The drug release behavior of cl-CMC-g-pHEA hydrogel was evaluated using a mathematical model. Based on the value of the correlation coefficient (R^2), the *in vitro* drug release of cl-CMC-g-pHEA hydrogels correlated better with the Higuchi model, a diffusion release system, than with the Hixson-Crowell model, an erosion release system. In order to

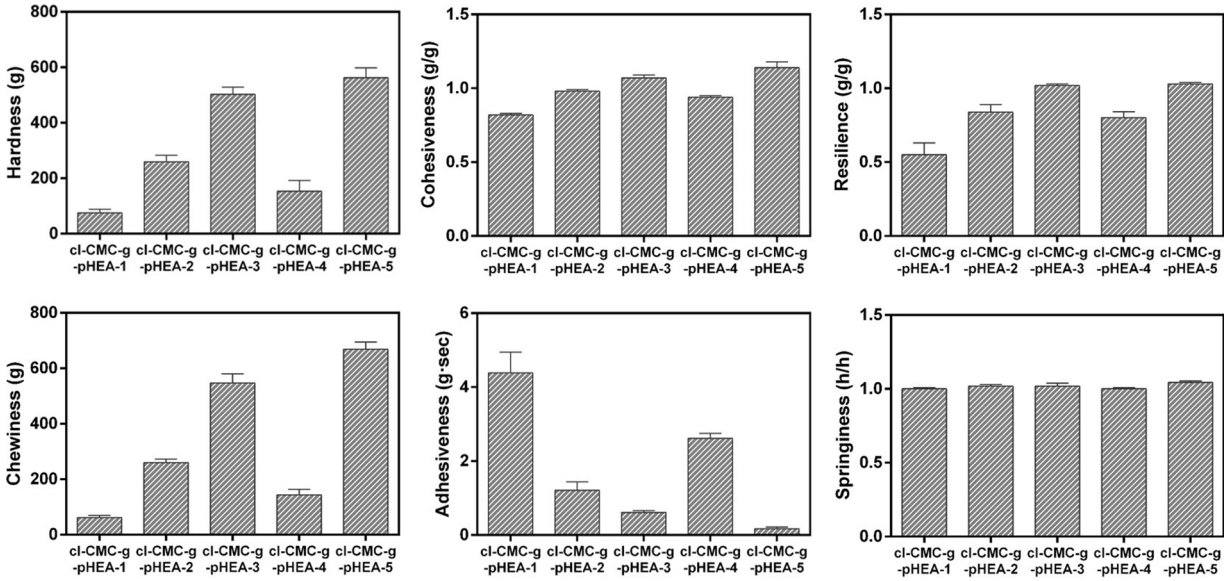

Fig. 6. Texture properties (hardness, cohesiveness, resilience, chewiness, adhesiveness, and springiness) of cl-CMC-g-pHEA hydrogels. Values are presented as mean ± SD (n = 3).

Table 2
Correlation coefficients (R^2) between release profiles and several kinetic models (first-order, Hixon-Crowell, and Higuchi) and the Korsmeyer-Peppas and Peppas-Sahlin model (release mechanism).

Release model	First Order	Hixson-Crowell	Higuchi		Korsmeyer-Peppas		Peppas-Sahlin		
	R^2	R^2	R^2	K_H	R^2	n	R^2	K_f	K_r
pH 5.5	0.2845	0.1027	0.8054	0.1042	0.9868	0.2453	0.9693	0.1587	−0.0132
pH 7.5	0.6012	0.4776	0.8506	0.1780	0.9810	0.2709	0.9632	0.2880	−0.0198
pH 8.5	0.6228	0.9219	0.9083	0.1598	0.9667	0.3518	0.9532	0.2256	−0.0102

investigate the release process more clearly, Korsmeyer-Peppas and Peppas-Sahlin models were used. The cl-CMC-g-pHEA hydrogels showed a high correlation with these models ($R^2 > 0.96$, $R^2 > 0.95$, respectively), indicating a significant analysis. Based on the Korsmeyer-Peppas ($n < 0.45$) and Peppas-Sahlin ($K_r < K_f$) equations, the dominant mechanism of drug release was Fickian diffusion. Furthermore, the diffusion constant K_f increased with increasing pH and the relaxation constant K_r was lower than K_f. These data indicate that, NRG release from a cl-CMC-g-pHEA hydrogel is governed by diffusion and that the rate of drug release can be adjusted according to skin pH (Table 2).

3.10. In vitro skin permeation

In order to confirm the possibility of using cl-CMC-g-pHEA as a transdermal delivery system, *in vitro* skin permeability was evaluated using a Franz diffusion cell. The control groups were prepared using 1,3-BG and 20% 1,3-BG (in PBS) for incorporation of NRG in the hydrogel. The results showed the drugs present in the stratum corneum (tape), in the epidermis except for the stratum corneum and dermis (skin), and in the receptor phase that had penetrated the dermis (transdermal) (Fig. 8). After 24 h, total permeation was 58.8% for cl-CMC-g-pHEA-4 hydrogel and was superior to 1,3-BG and 20% 1,3-BG/PBS (43.5 and 42.4%, respectively). For the 1,3-BG solution sample, the largest amount of NRG was present in the stratum corneum because it was difficult to penetrate through the skin with 1,3-BG solution only; thus, it remained in the stratum corneum. In the 20% BG/PBS sample, the amount of drug in the stratum corneum decreased and that penetrating the dermis (transdermal) increased because most active ingredients could travel through the pores. Penetration through pores could occur more easily when PBS was added to reduce the viscosity of 1,3-BG. In the cl-CMC-g-pHEA sample, the amount of drug present in the epidermis and the dermis was slightly different than that in the control group, but the amount that penetrated into the dermis increased drastically. The hydrogel seals the surface of the skin to promote hydration, thereby, improving the diffusion of the drug. This result suggests that the hydrated stratum corneum temporarily interferes with the barrier function of the skin and that the active ingredient incorporated into the hydrogel easily crosses into the skin.

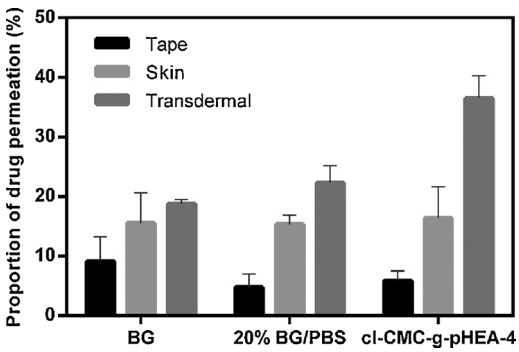

Fig. 8. Proportions of permeated NRG in 1,3-butylene glycol (BG), 20% 1,3-BG/phosphate buffer solution (PBS) and cl-CMC-g-pHEA-4 after 24 h. (Tape: stratum corneum, Skin: epidermis without stratum corneum and dermis, Transdermal: permeated through the skin). Values are presented as mean ± SD (n = 3).

3.11. Drug stability

The stability of cl-CMC-g-pHEA-4 hydrogel as an NRG carrier was examined. Drug-release characteristics of NRG-loaded hydrogel was measured before and after the 30-day stability study (see Fig. S7). It was evident that the formulation remained stable at 40 °C and 75% RH for up to 30 days. Thus, it can be considered as an excellent carrier for NRG.

4. Conclusion

In this study, we synthesized a pH-responsive hydrogel from CMC and 2-HEA in order to develop a transdermal delivery system for NRG, a drug for treatment of atopic skin conditions. Destruction of the acid mantle on the skin surface causes several skin diseases, such as the atopic skin, the pH of the skin changes to 7-9. Hydrogel synthesis was confirmed by FT-IR and ^{1}H NMR. The SEM images of cl-CMC-g-pHEA hydrogels showed a 3D-network structure, which allows the drug to diffuse out of the gel. A difference in the water loss amount of up to 16% was found between the hydrogels at 100 °C by TGA (maximum water loss of cl-CMC-g-pHEA-5: -95.3%, minimum water loss of cl-CMC-g-pHEA-1: -79.2%). The swelling ratio of the hydrogel increased as the grafting and the crosslinking density decreased, and at pH 7.5 and 8.5. This result was due to the electrostatic repulsive force generated by the ionization of the carboxyl groups. Rheological characteristics, including hardness, cohesiveness, resilience, chewiness, adhesiveness, and springiness were analyzed to determine the optimal properties of hydrogels for use as transdermal delivery systems. The NRG release behavior of cl-CMC-g-pHEA-4 dominantly followed Fickian diffusion mechanisms. An *in vitro* skin permeation study showed that cl-CMC-g-pHEA hydrogel improved skin penetration of NRG. Taken together, these results show that the hydrogel hydrates the skin, which temporarily interferes with the barrier function of the skin and allows the drug to penetrate the skin. In conclusion, a novel cl-CMC-g-pHEA hydrogel is an effective transdermal delivery system for treatment of various skin lesions caused by pH imbalance and may be effectively used as a smart hydrogel.

Conflicts of interest

The authors have no conflict of interest to declare.

Acknowledgments

This work was supported by the Industry-University-Research Cooperation Technology Development Project (C0541175) of the Small and Medium Business Administration of Korea.

Appendix A. Supplementary data

Supplementary material related to this article can be found, in the online version, at doi:https://doi.org/10.1016/j.carbpol.2018.08.011.

References

Anirudhan, T. S., Sandeep, S., & Divya, P. L. (2012). Synthesis and characterization of maleated cyclodextrin-grafted-silylated montmorillonite for the controlled release and colon specific delivery of tetracycline hydrochloride. *RSC Advances, 2*, 9555–9564.

Anseth, K. S., Bowman, C. N., & Brannon-Peppas, L. (1996). Mechanical properties of hydrogels and their experimental determination. *Biomaterials, 17*(17), 1647–1657.

Arunbabu, D., Shahsavan, H., Zhang, W., & Zhao, B. (2013). Poly(AAc-*co*-MBA) hydrogel films: Adhesive and mechanical properties in aqueous medium. *The Journal of Physical Chemistry B, 117*(1), 441–449.

Bisht, S. S., Pandey, K. K., Joshi, G., & Naithani, S. (2017). New route for carboxymethylation of cellulose: Synthesis structural analysis and properties. *Cellulose Chemistry and Technology, 51*, 609–619.

Boateng, J. S., Matthews, K. H., Stevens, H. N., & Eccleston, G. M. (2008). Wound healing dressings and drug delivery systems: A review. *Journal of Pharmaceutical Sciences, 97*(8), 2892–2923.

Bonacucina, G., Martelli, S., & Palmieri, G. F. (2004). Rheological, mucoadhesive and release properties of Carbopol gels in hydrophilic cosolvents. *International Journal of Pharmaceutics, 282*(1-2), 115–130.

Chan, Y., Wong, T., Byrne, F., Kavallaris, M., & Bulmus, V. (2008). Acid-labile core cross-linked micelles for pH-triggered release of antitumor drugs. *Biomacromolecules, 9*(7), 1826–1836.

Chen, D., Chen, M. S., Cui, Q. C., Yang, H., & Dou, Q. P. (2007). Structure-proteasome-inhibitory activity relationships of dietary flavonoids in human cancer cells. *Frontiers in Bioscience, 12*, 1935–1945.

Das, D., & Pal, S. (2015). Dextrin/poly (HEMA): pH responsive porous hydrogel for controlled release of ciprofloxacin. *International Journal of Biological Macromolecules, 72*, 171–178.

Das, D., Ghosh, P., Dhara, S., Panda, A. B., & Pal, S. (2015). Dextrin and poly(acrylic acid)-based biodegradable, non-cytotoxic, chemically cross-linked hydrogel for sustained release of ornidazole and ciprofloxacin. *ACS Applied Materials & Interfaces, 7*(8), 4791–4803.

Das, D., Pham, T. T. H., & Noh, I. S. (2018). Characterizations of hyaluronate-based terpolymeric hydrogel synthesized via free radical polymerization mechanism for biomedical applications. *Colloids and Surfaces B, Biointerfaces, 170*, 64–75.

Dash, S., Murthy, P. N., Nath, L., & Chowdhury, P. (2010). Kinetic modeling on drug release from controlled drug delivery systems. *Acta Poloniae Pharmaceutica, 67*(3), 217–223.

Demirdirek, B., & Uhrich, K. E. (2017). Novel salicylic acid-based chemically crosslinked pH-sensitive hydrogels as potential drug delivery systems. *International Journal of Pharmaceutics, 528*(1-2), 406–415.

Devi, N., & Narzary, A. (2012). Release dynamics of brufen from a drug loaded polymer hydrogel containing polyvinyl alcohol, 2-acrylamide-2-methylpropane sulfonic acid and acrylamide. *International Journal of Polymeric Materials, 61*, 821–833.

Dobić, S. N., Filipović, J. M., & Tomić, S. L. (2012). Synthesis and characterization of poly (2-hydroxyethyl methacrylate/itaconic acid/poly (ethylene glycol) dimethacrylate) hydrogels. *Chemical Engineering Journal, 179*, 372–380.

Dorkoosh, F. A., Verhoef, J. C., Borchard, G., Rafiee-Tehrani, M., Verheijden, J. H., & Junginger, H. E. (2002). Intestinal absorption of human insulin in pigs using delivery systems based on superporous hydrogel polymers. *International Journal of Pharmaceutics, 247*(1-2), 47–55.

Ganji, F., Vasheghani-Farahani, S., & Vasheghani-Farahani, E. (2010). Theoretical description of hydrogel swelling: A review. *Iran Polymer Journal, 19*(5), 375–398.

Guo, B., Wistrand, A. F., & Albertsson, A. C. (2011). Facile synthesis of degradable and electrically conductive polysaccharide hydrogels. *Biomacromolecules, 12*(7), 2601–2609.

Hu, X., Wang, Y., Zhang, L., Xu, M., Dong, W., & Zhang, J. (2017). Fabrication of Salecan/poly(AMPS-co-HMAA) semi-IPN hydrogels for cell adhesion. *Carbohydrate Polymers, 174*, 171–181.

Hurler, J., Engesland, A., Kermany, B. P., & Škalko-Basnet, N. (2012). Improved texture analysis for hydrogel characterization: Gel cohesiveness, adhesiveness, and hardness. *Journal of Applied Polymer Science, 125*(1), 180–188.

Jones, D. S., Woolfson, A. D., & Brown, A. F. (1997). Textural, viscoelastic and mucoadhesive properties of pharmaceutical gels composed of cellulose polymers. *International Journal of Pharmaceutics, 151*(2), 223–233.

Karuppaqounder, V., Arumugam, S., Thandavarayan, R. A., Sreedhar, R., Giridharan, V. V., Pitchaimani, V., et al. (2016). Naringenin ameliorates skin inflammation and accelerates phenotypic reprogramming from M1 to M2 macrophage polarization in atopic dermatitis NC/Nga mouse model. *Experimental Dermatology, 25*(5), 404–407.

Kawaii, S., Tomono, Y., Katase, E., Ogawa, K., & Yano, M. (1999). HL-60 differentiating activity and flavonoid content of the readily extractable fraction prepared from citrus juices. *Journal of Agricultural and Food Chemistry, 47*(1), 128–135.

Kim, T. H., Kim, G. D., Ahn, H. J., Cho, J. J., Park, Y. S., & Park, C. S. (2013). The inhibitory effect of naringenin on atopic dermatitis induced by DNFB in NC/Nga mice. *Life Science, 93*(15), 516–524.

Kim, A. R., Park, H. S., Kim, S. S., & Noh, I. S. (2013). Biological evaluation of cellulose hydrogel with temperature-responsive particles. *Biomaterials Research, 17*, 181–186.

Koehler, J., Wallmeyer, L., Hedtrich, S., Goepferich, A. M., & Brandl, F. P. (2017). pH-Modulating poly(ethylene glycol)/alginate hydrogel dressings for the treatment of chronic wounds. *Macromolecular Bioscience, 17*(5), 1600369–1600380.

Kong, B. J., Kim, A., & Park, S. N. (2016). Properties and in vitro drug release of hyaluronic acid-hydroxyethyl cellulose hydrogels for transdermal delivery of isoliquiritigenin. *Carbohydrate Polymers, 147*, 473–481.

Korsmeyer, R. W., Gurny, R., Doelker, E., Buri, P., & Peppas, N. A. (1983). Mechanisms of solute release from porous hydrophilic polymers. *International Journal of Pharmaceutics, 15*, 25–35.

Kwon, S. S., Kong, B. J., & Park, S. N. (2015). Physicochemical properties of pH-sensitive hydrogels based on hydroxyethyl cellulose-hyaluronic acid and for applications as transdermal delivery systems for skin lesions. *European Journal of Pharmaceutics and Biopharmaceutics, 92*, 146–154.

Ladenheim, D., Martin, G. P., Marriott, C., Hollingsbee, D. A., & Brown, M. B. (1996). An in-vitro study of the effect of hydrocolloid patch occlusion on the penetration of triamcinolone acetonide through skin in man. *The Journal of Pharmacy and Pharmacology, 48*(8), 806–811.

Liu, P., Zhai, M., Li, J., Peng, J., & Wu, J. (2002). Radiation preparation and swelling behavior of sodium carboxymethyl cellulose hydrogels. *Radiation Physics and Chemistry, 63*(3-6), 525–528.

Mandal, B., Rameshbabu, A. P., Dhara, S., & Pal, S. (2017). Nanocomposite hydrogel derived from poly (methacrylic acid)/carboxymethyl cellulose/AuNPs: A potential transdermal drugs carrier. *Polymer, 120*, 9–19.

Mandalari, G., Bisignano, C., D'Arrigo, M., Ginestra, G., Arena, A., Tomaino, A., et al. (2010). Antimicrobial potential of polyphenols extracted from almond skins. *Letters in Applied Microbiology, 51*(1), 89–93.

Martin, G. P., Ladenheim, D., Marriott, C., Hollingsbee, D. A., & Brown, M. B. (2000). The influence of hydrocolloid patch composition on the bioavailability of triamcinolone acetonide in humans. *Drug Development and Industrial Pharmacy, 26*(1), 35–43.

Martínez-Ramos, C., Lainez, S., Sancho, F., García Esparza, M. A., Planells-Cases, R., García Verdugo, J. M., et al. (2008). Differentiation of postnatal neural stem cells into glia and functional neurons on laminin-coated polymeric substrates. *Tissue Engineering Part A, 14*(8), 1365–1375.

Mauro, T., Holleran, W. M., Grayson, S., Gao, W. N., Man, M. Q., & Kriehuber, E. (1998). Barrier recovery is impeded at neutral pH, independent of ionic effects: implications for extracellular lipid processing. *Archives of Dermatological Research, 290*(4), 215–222.

Michaels, A. S., Chandrasekaran, S. K., & Shaw, J. E. (1975). Drug permeation through human skin: Theory and in vitro experimental measurement. *AIChE Journal, 21*(5), 985–996.

Moon, P. D., Choi, I. H., & Kim, H. M. (2011). Naringenin suppresses the production of thymic stromal lymphopoietin through the blockade of RIP2 and caspase-1 signal cascade in mast cells. *European Journal of Pharmacology, 671*(1-3), 128–132.

Otto, D. P., & De Villiers, M. M. (2014). What is the future of heated transdermal delivery systems? *Therapeutic Delivery, 5*(9), 961–964.

Park, K. R., & Nho, Y. C. (2003). Synthesis of PVA/PVP hydrogels having two-layer by radiation and their physical properties. *Radiation Physics and Chemistry, 67*, 361–365.

Park, H. Y., Kim, G. Y., & Chio, Y. H. (2012). Naringenin attenuates the release of pro-inflammatory mediators from lipopolysaccharide-stimulated BV2 microglia by inactivating nuclear factor-κB and inhibiting mitogen-activated protein kinases. *International Journal of Molecular Medicine, 30*(1), 204–210.

Park, S. H., Shin, H. S., Yun, M. E., Lee, S. L., Song, B. R., Lee, N. H., et al. (2018). Physical characterization and in vitro skin permeation of elastic liposomes loaded with kaempferol and nicotiflorin. *Polymer-Korea, 42*(2), 330–338.

Pasqui, D., De Cagna, M., & Barbucci, R. (2012). Polysaccharide-based hydrogels: The key role of water in affecting mechanical properties. *Polymers, 4*(3), 1517–1534.

Patra, P., Seesala, V. S., Das, D., Panda, A. B., Dhara, S., & Pal, S. (2018). Biopolymeric nanogel derived from functionalized glycogen towards targeted delivery of 5-fluorouracil. *Polymer, 140*, 122–130.

Peppas, N. A., & Hoffman, A. S. (2013). Hydrogels. In D. R. Buddy, A. S. Hoffman, F. J. Schoen, & J. E. Lemons (Eds.). *Biomaterials science* (pp. 35). United States: Academic Press Chapter 1.

Peppas, N. A., & Sahlin, J. J. (1989). A simple equation for the description of solute release. III. Coupling of diffusion and relaxation. *International Journal of Pharmaceutics, 52*, 169–172.

Puranik, A. S., Pao, L. P., White, V. M., & Peppas, N. A. (2016). Synthesis and characterization of pH-responsive nanoscale hydrogels for oral delivery of hydrophobic therapeutics. *European Journal of Pharmaceutics and Biopharmaceutics, 108*, 196–213.

Rauha, J. P., Remes, S., Heinonen, M., Hopia, A., Kähkönen, M., Kujala, T., et al. (2000). Antimicrobial effects of Finnish plant extracts containing flavonoids and other phenolic compounds. *International Journal of Food Microbiology, 56*(1), 3–12.

Santa-Comba, A., Pereira, A., Lemos, R., Santos, D., Amarante, J., Pinto, M., et al. (2001). Evaluation of carboxymethyl cellulose, hydroxypropylmethyl cellulose, and aluminum hydroxide as potential carriers for rhBMP-2. *Journal of Biomedical Materials Research Part A, 55*(3), 396–400.

Tobing, S. D., & Klein, A. (2001). Molecular parameters and their relation to the adhesive performance of acrylic pressure-sensitive adhesives. *Journal of Applied Polymer Science, 79*(12), 2230–2244.

Wach, R. A., Mitomo, H., Nagasawa, N., & Yoshii, F. (2003). Radiation crosslinking of carboxymethyl cellulose of various degree of substitution at high concentration in aqueous solutions of natural pH. *Radiation Physics and Chemistry, 68*(5), 771–779.

Wang, Y. Y., Hong, C. T., Chiu, W. T., & Fang, J. Y. (2001). In vitro and in vivo evaluations of topically applied capsaicin and nonivamide from hydrogels. *International Journal of Pharmaceutics, 224*(1-2), 89–104.

Wei, W., Hu, X., Qi, X., Yu, H., Liu, Y., Li, J., et al. (2015). A novel thermo-responsive hydrogel based on salecan and poly(*N*-isopropylacrylamide): Synthesis and characterization. *Colloids and Surfaces B, Biointerfaces, 144*, 99–107.

Weian, Z., Wei, L., & Yue'e, F. (2005). Synthesis and properties of a novel hydrogel nanocomposites. *Materials Letters, 59*(23), 2876–2880.

Xiao, C., & Gao, Y. (2008). Preparation and properties of physically crosslinked sodium carboxymethyl cellulose/poly(vinyl alcohol) complex hydrogels. *Journal of Applied Polymer Science, 107*(3), 1568–1572.

Xu, X., Shen, Y., Wang, W., Sun, C., Li, C., Xiong, Y., et al. (2014). Preparation and in vitro

characterization of thermosensitive and mucoadhesive hydrogels for nasal delivery of phenylephrine hydrochloride. *European Journal of Pharmaceutics and Biopharmaceutics, 88*(3), 998–1004.

Yáñez-S, M., Matsuhiro, B., Maldonado, S., González, R., Luengo, J., Uyarte, O., et al. (2018). Carboxymethylcellulose from bleached organosolv fibers of Eucalyptus nitens: Synthesis and physicochemical characterization. *Cellulose, 25*(5), 2901–2914.

Yao, X., Chen, L., Chen, X., Zhang, Z., Zheng, H., He, C., et al. (2014). Intracellular pH-sensitive metallo-supramolecular nanogels for anticancer drug delivery. *ACS Applied Materials & Interfaces, 6*(10), 7816–7822.

Yu, S., Zhang, X., Tan, G., Tian, L., Liu, D., Liu, Y., et al. (2017). A novel pH-induced thermosensitive hydrogel composed of carboxymethyl chitosan and poloxamer cross-linked by glutaraldehyde for ophthalmic drug delivery. *Carbohydrate Polymers, 155*(2), 208–217.

Zhang, X., Yang, D., & Nie, J. (2008). Chitosan/polyethylene glycol diacrylate films as potential wound dressing material. *International Journal of Biological Macromolecules, 43*(5), 456–462.

Zhong, C., Wu, J., Reinhart-King, C. A., & Chu, C. C. (2010). Synthesis, characterization and cytotoxicity of photo-crosslinked maleic chitosan-polyethylene glycol diacrylate hybrid hydrogels. *Acta Biomaterialia, 6*(10), 3908–3918.

Zuidema, J. M., Rivet, C. J., Gilbert, R. J., & Morrison, F. A. (2014). A protocol for rheological characterization of hydrogels for tissue engineering strategies. *Journal of Biomedical Materials Research Part B, Applied Biomaterials, 102*(5), 1063–1073.